IEEE Access
Multidisciplinary | Rapid Review | Open Access Journal

Received August 8, 2020, accepted August 28, 2020, date of publication September 2, 2020, date of current version September 15, 2020.

Digital Object Identifier 10.1109/ACCESS.2020.3021124

Clutter Suppression and Target Tracking by the Low-Rank Representation for Airborne Maritime Surveillance Radar

CHENGHUI CAO[1,2,3,4], JIE ZHANG[2,4], JUNMIN MENG[2,4], (Member, IEEE), XI ZHANG[2,4], (Member, IEEE), AND XINGPENG MAO[1,3], (Member, IEEE)

[1]School of Electronics and Information Engineering, Harbin Institute of Technology, Harbin 150001, China
[2]Ministry of Natural Resources, First Institute of Oceanography, Qingdao 266061, China
[3]Ministry of Industry and Information Technology, Key Laboratory of Marine Environmental Monitoring and Information Processing, Harbin 150001, China
[4]Ministry of Natural Resources, Ocean Telemetry Technology Innovation Center, Qingdao 266061, China

Corresponding author: Xingpeng Mao (mxp@hit.edu.cn)

This work was supported in part by the National Key Research and Development Program of China under Grant 2017YFC1405201, in part by the National Natural Science Foundation of China under Grant 61971455, and in part by the National Pre-Research Foundation under Grant 61404160109.

ABSTRACT Moving target detection is of vital importance to maritime security and maritime resource protection. However, the detection of slow or weak targets is difficult based on traditional methods. A new detection method is proposed by using the different motion variations of radar moving target and sea clutter in the range-Doppler spectrum sequence. The first step in implementing this method is the separation of moving target and sea clutter by the low-rank representation, in which the target and clutter are modeled as foreground and background components. Subsequently, a sea clutter discriminator is constructed within the sea clutter bandwidth to further remove the sea clutter (false alarms) that exists in the foreground. The proposed method can reduce the sea clutter power while maintaining the target power and improve the detection rate of moving targets, especially slow or weak targets. Data collected with airborne maritime surveillance radar in maritime moving target indication (MMTI) mode are used to validate the performance of the proposed method. The experimental results demonstrate that the improvement in the signal-to-clutter ratio (SCR) obtained with the proposed method is better than that obtained with space-time adaptive processing (STAP, including 1DT-STAP, 3DT-STAP and sparse-STAP) and principal component pursuit (PCP) methods; additionally, the figure of merit (*FOM*) of the proposed method is higher than that of the constant false alarm rate (CFAR) and PCP method. Furthermore, the tracks of ships are obtained by applying a location constraint to the foreground sequence.

INDEX TERMS Clutter suppression, low-rank representation, range-Doppler sequence, sea clutter discriminator, target detection and tracking.

I. INTRODUCTION

Airborne maritime surveillance radar can achieve the long-range, wide-range and multi-angle detection of moving targets based on the periodic azimuth scanning of radar antennas [1], which can expand the scope of maritime surveillance without increasing the cruise time and frequency, and has become an important means of maritime target detection [2].

At present, airborne maritime surveillance radar has been widely used in both the military and civil fields [3], [4]. Military operations mainly include anti-ship and anti-submarine over-the-horizon target indications, as well as moving target detection for coastal areas and reef surfaces. The civil use mainly includes maritime search and rescue, anti-smuggling, illegal immigration control, fishery management and marine resource protection [5]. Since the 1960s, many airborne maritime surveillance radar systems have been developed, such as the American AN/APY-10, AN/ZPY-3 and SeaVue radar, the French Ocean Master radar, Israel's EL/M-2022A/H/U radar, and the European Seaspray series AESA radar [6]–[9]. These radar systems all support maritime moving target indication (MMTI) mode, which can be applied for a wide range of maritime target detection and tracking tasks [10]–[12].

The associate editor coordinating the review of this manuscript and approving it for publication was Chuan Li.

With the development of airborne maritime surveillance systems, a series of methods have been proposed for maritime moving target detection by utilizing the energy difference between radar target and sea clutter. Among which, sea clutter [13] is an echo that is backscattered from the ocean surface after being irradiated by radar signals, which seriously influence the maritime target detection for its high power. Its existence seriously interferes with the detection and tracking performance of radar targets on the sea surface These methods mainly involve the combination of traditional moving target detection (MTD) and adaptive detection technology, among which, space-time adaptive processing (STAP) [14] and constant false alarm rate (CFAR) detection are classic methods of clutter suppression and target detection, respectively, and many results have achieved the detection of large-size and high-strength targets [15]–[18]. For example, Yu *et al.* [19] proposed an adaptive dual-threshold sparse Fourier transform (ADT-SFT) algorithm, and experiments demonstrated that the ADT-SFT algorithm is more suitable for the clutter background and can obtain a better detection performance than SFT and robust SFT. Magraner *et al.* [20] presented a new technique based on cell-averaging CFAR detection, and it achieved good detection results. Wang *et al.* [21] proposed a novel subspace STAP algorithm by combining the conventional method and augmented subspace, and the numerical results demonstrated that the proposed algorithm has a superior performance in a finite-training-sample situation. Although much work has been done, the detection of slow or weak targets is still difficult. On the one hand, slow or weak targets are often submerged in the sea clutter bandwidth due to the serious Doppler broadening of sea clutter with the movement of aircraft and ship targets, resulting in serious performance degradation for the corresponding methods [22], [23]. On the other hand, the slow target echo is located in the main sea clutter region of the Doppler domain; hence, moving target indication (MTI)-based sea clutter suppression reduces not only the energy of sea clutter, but also the energy of the target echo [24], resulting in a low detection rate for targets, especially weak or slow targets. Furthermore, the traditional methods rely on accurate statistical models of clutter and target echo. With the improvement of radar resolution, sea clutter becomes increasingly complex (non-stationary in time, heterogeneous in space, and non-Gaussian in the probability distribution), and the frequency of sea peaks increases; hence, it is difficult to accurately model these processes, resulting in a high false alarm.

To solve the problems of traditional methods, some new methods have been proposed by researchers, such as methods based on sea surface fractal characteristics, time-frequency analysis and neural networks. The methods based on sea surface fractal features are simple and high efficiency. Li *et al.* [25] combined empirical mode decomposition and the multifractal characteristics of sea clutter signals to detect targets, and the results show that the proposed method is better than the generalized Hurst exponent. Du [26] proposed a novel method for detecting radar targets based on the fractal characteristics of sea-surface scattering, in which the fractional Brownian motion model is used. The experiments show that the method is reliable and can improve the accuracy of detection. However, the fractal characteristics of a sea clutter time series only exist in a certain time interval, which varies with the change of radar parameters, sea state and polarization. When the observation time is short, the performance of the detector will seriously decline [27]. For the method based on time-frequency analysis, information can be extracted from the time domain and frequency domain at the same time by appropriate time-frequency transform. To improve the detection rate of sea-surface targets, Shi and Shui [28] utilized the time-frequency difference of targets and sea clutter to improve the detection rate in integration time of the order of seconds. Shui *et al.* [29] proposed a new range-spread target detection scheme exploiting the image features of cross time-frequency distribution of a pair of adjacent received signals. The proposed algorithm is verified by using raw radar data and outperforms the conventional detection methods. However, the contradiction between the temporal resolution and frequency resolution results in many challenges in terms of long-range target detection [30], [31]. By using big data to train neural network detectors, the method based on neural networks can extract multiple potential features, thus overcoming the problem of excessive human intervention. Wang *et al.* [32] constructed a convolutional neural network (CNN) detector for radar target detection, and the CNN detector has a better performance than the CFAR detector when the SNR of the target is large. Liu *et al.* [33] proposed a novel deep convolutional neural network (CNN)-based method for the MTI (CNN-MTI), and the simulation results demonstrated the validity and the robustness of the CNN-MTI in a non-homogeneous and low SCR environment. However, the design of the detector depends on both the samples of target and clutter, and the number of sea clutter samples is generally far greater than that of target samples; hence, the imbalance between target and clutter samples decreases the detector capacity [34].

Overall, although the existing methods mentioned above have achieved good detection results in some specific environments, they are unable to self-adapt to changes in the environment. With the effects of the radar resolution, wind, wave and current, as well as the incidence angle, the existing methods have poor robustness, making it difficult to detect slow or weak targets. Therefore, new methods for suppressing sea clutter and detecting moving targets must be urgently developed.

In recent years, methods based on the low-rank and sparse matrix separation is developed. The low-rank and sparse matrix separation has been successfully applied in many fields, such as image noise reduction [35], keyword extraction [36], image alignment [37], clutter suppression of wall-through radars [38] and target detection [4]. Specially, Yan *et al* [4] presented a novel approach for extracting moving targets by using the multi-channel radar data based

on the method of principal component pursuit (PCP) [39], the multi-channel radar system has good spatial consistency, but the system complexity is high and the cost is expensive. In this paper, based on the method of DECOLOR (DEtecting Contiguous Outliers in the LOw-rank Representation) in [40], a method of sea clutter suppression and moving target tracking with the low-rank representation is proposed by using the different motion behavior of the target and clutter in range-Doppler spectrum sequence. The proposed method is applicable to common airborne wide area surveillance radar and can reduce the sea clutter power while maintaining the target power, then subsequently improve the detection performance of moving targets, especially for slow or weak targets.

The structure of this paper is as follows. Section II describes the proposed method in detail. Section III presents the application of the proposed method to airborne maritime surveillance radar, including an introduction of experimental data, the performance of sea clutter suppression and target detection, and the result of the target tracking. Section IV is the conclusion.

II. METHOD

This section discusses the details of the proposed method for clutter suppression and target detection. By utilizing the different motion characteristics of target and clutter in a range-Doppler spectrum sequence, including the range and velocity (radial Doppler velocity and the variation in the velocity), the separation between the radar target and sea clutter can be represented as a problem of detecting contiguous outliers in the low-rank representation. In this case, the radar target can be modeled as the foreground and sea clutter as the background, hence, the stationary sea clutter is suppressed. Considering that part of the background energy (sea clutter) is leaked into the foreground (target), a sea clutter discriminator is constructed to remove the sea clutter from the foreground by defining the foreground and background frequencies. Therefore, the locations and tracks of targets are obtained. The framework of this method is shown in Fig. 1, including sea clutter suppression, target detection and target tracking with the low-rank representation.

A. LOW-RANK REPRESENTATION IN RADAR

Considering the low-rank and sparse characteristics of sea clutter and targets in the range-Doppler spectrum sequence, sea clutter and targets can be separated by utilizing their different motion behaviors. Consequently, radar target is modeled as the foreground and sea clutter is modeled as the background in the range-Doppler sequence.

1) RANGE-DOPPLER SPECTRUM SEQUENCE GENERATION

The 3D geometry of the airborne maritime surveillance radar is shown in Fig. 2. The plane velocity is V and its altitude is H. The X-axis is parallel to the direction of V, and the Y-axis is perpendicular to the X-axis. Assuming that a point P is located on the ground, the azimuth angle is θ (the fuselage is positive to the right, and negative to the left), the pitching angle is φ, and the initial slant distance is R_1. As the plane flies, the antenna continuously scanned periodically to achieve a wide surveillance range.

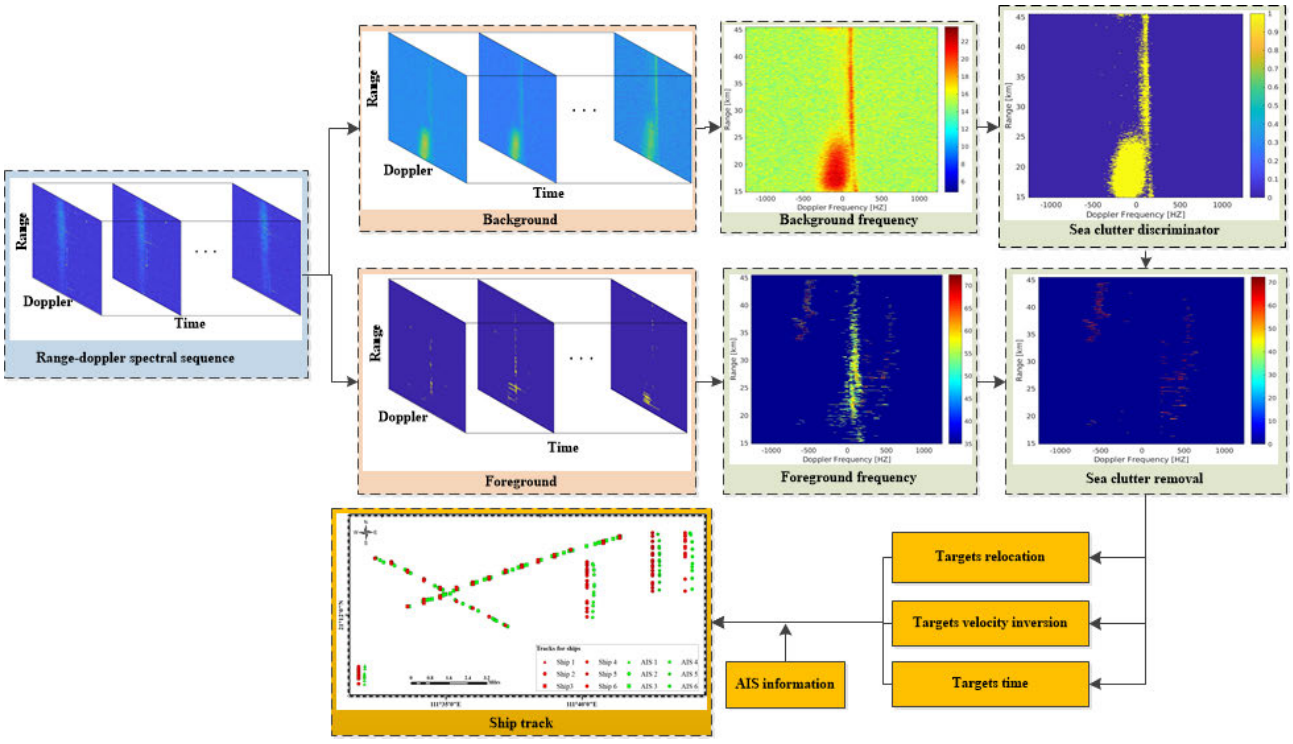

FIGURE 1. The framework of the proposed method.

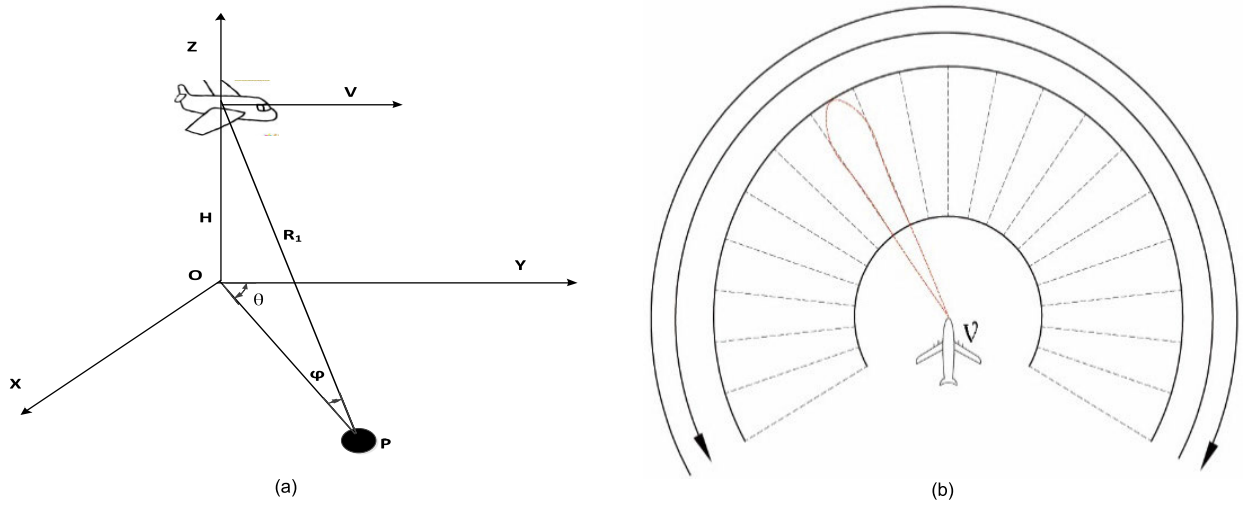

FIGURE 2. Geometry of the airborne maritime surveillance radar. (a) 3D geometry of radar. (b) Periodic scanning of radar antenna.

The transmitted signal is assumed to be a linear frequency-modulated (LFM) signal

$$E(\tau) = \text{rect}(\frac{\tau}{T_p}) \exp[j2\pi(f_c\tau + \frac{\eta}{2}\tau^2)] \tag{1}$$

where rect $(\cdot)$ is the unit rectangular function, τ denotes the fast time, T_p denotes the pulse width, f_c is the carrier frequency, and η is the chirp rate. The returned signal is

$$S'(\tau, t) = \sigma \cdot \text{rect}(\tau - \frac{2R(t)}{c} \Big/ T_\text{p}) \cdot \exp\{j2\pi[f_c(\tau - \frac{2R(t)}{c}) + \frac{\eta}{2}(\tau - \frac{2R(t)}{c})^2]\} \tag{2}$$

where t denotes the slow time, σ is the function of the backward scattering coefficient, and c is the velocity of light.

According to the 3D geometry of radar detection, the instantaneous slant range between the scattering center and the radar can be written as

$$R(t) \approx R_1 - Vt\cos\theta\cos\varphi \tag{3}$$

The Doppler centroid frequency is given as

$$f_\text{d} = \frac{2V\cos\theta\cos\varphi}{\lambda} \tag{4}$$

where λ is the wavelength. Assuming that θ_0 is the center azimuth angle of the radar beam, and $\Delta\theta$ is the 3 dB azimuth beam width. The Doppler bandwidth can be calculated as

$$\Delta f_\text{d} = \left| f_d(\theta_0 - \frac{\Delta\theta}{2}) - f_d(\theta_0 + \frac{\Delta\theta}{2}) \right| = \frac{2V\sin\theta_0\cos\varphi}{\lambda}\Delta\theta \tag{5}$$

After range compression and range cell migration correction (RCMC) [41], [42], the received signal becomes

$$S''(\tau, t) = \sigma \cdot rect(\frac{t}{T_\text{a}}) \sin c[B_1(\tau - \frac{2R_1}{c})] \exp(-j4\pi\frac{R(t)}{\lambda}) \tag{6}$$

where $T_\text{a} = N_0 t_r$ is the coherent processing interval (CPI), t_r is the pulse repetition interval (PRI), and N_0 is the number of pulses in one CPI. The symbol B_1 represents the bandwidth of the transmitted signal. By using the Fourier transform (FFT) for the slow time t, the range-Doppler spectrum is obtained as

$$x(\tau, f) = FFT(S''(\tau, t)) \tag{7}$$

where f is the Doppler frequency.

As shown in Fig. 3, the same area on the sea surface will be scanned by the radar antenna in multiple periods. Combined with radar beam pointing, velocity, latitude and longitude of airplane and slant range, the latitude and longitude of the four corners of each range-Doppler image can be calculated. The scanning velocity of antenna is fast on the wide sea surface area; hence the overlap between adjacent scan periods is very high, we try to keep the latitude and longitude of the four corners of each image in the range-Doppler sequence same, which can ensure the consistency of different images. Although not strictly accurate, the high overlap and the continuous Doppler spectrum characteristic ensure the low-rank property of the background. Furthermore, sea clutter changes slowly on wide sea surface area. Therefore, the error has very little effect on the subsequent detection, which is also demonstrated by the results in section III B. Therefore, for a certain area on the sea surface, the corresponding range-Doppler spectrum can be extracted as the spectrum sequence

$$X(r, d, n) = [x_1(\tau, f), x_2(\tau, f) \ldots x_\text{N}(\tau, f)] \tag{8}$$

where r, d and n represent the range bin, the Doppler bin and the sequence number, respectively. If the number of range bins is R_0, the number of Doppler bins is D_0, and the sequence number is N, so we have $X \in \Re^{Q\times N}$ and $Q = R_0 \times D_0$.

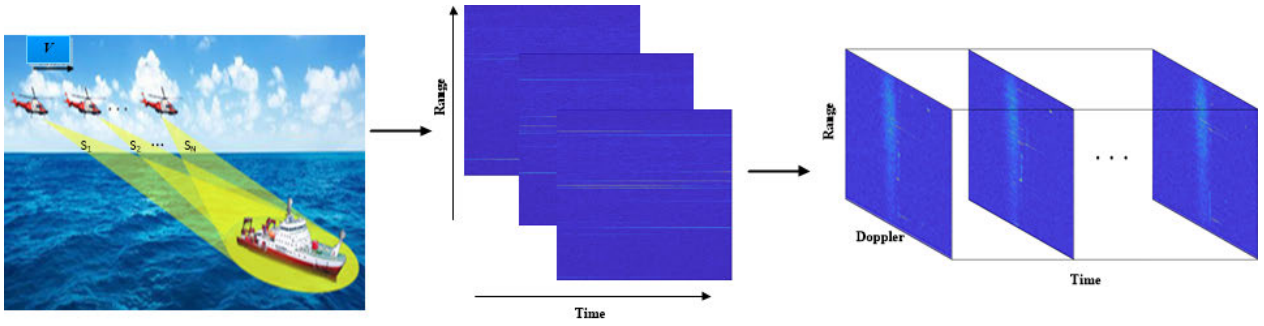

FIGURE 3. The generation of range-Doppler spectrum sequence from raw radar echo.

2) LOW-RANK REPRESENTATION OF SEA CLUTTER

In a short period, the sea clutter in the same region changes on a small scale and has low-rank characteristics, while the number of moving targets is sparse on a large sea area. In this section, sea clutter and targets are modeled based on the characteristics of low-rank and sparse, respectively. The objective function is constructed to obtain the clutter background and target foreground by optimizing the solution.

Assuming that $X = [x_1, x_2, \ldots, x_N] \in \Re^{Q\times N}$ represents a range-Doppler spectrum sequence with N frames, $x_n \in \Re^{Q}$ denotes the nth frame, and the qth pixel of frame n is denoted as qn. $B = [B_1, B_2, \ldots, B_N] \in \Re^{Q\times N}$ represents the corresponding background, and $S = [S_1, S_2, \ldots, S_N] \in \{0, 1\}^{Q\times N}$ is a binary matrix denoting the foreground support.

$$S_{qn} = \begin{cases} 0, & \text{if } qn \text{ is background} \\ 1, & \text{if } qn \text{ is foreground} \end{cases} \tag{9}$$

$P_S(X)$ represents the orthogonal projection of a matrix X onto the linear space of matrices supported by S,

$$p_S(X)(q,n) = \begin{cases} 0, & S_{qn} = 0 \\ X_{qn}, & S_{qn} = 1 \end{cases} \tag{10}$$

and $p_{S^\perp}(X)$ is its complementary projection. Then, we have $p_S(X) + p_{S^\perp}(X) = X$

In the range-Doppler spectrum sequence, we model radar targets as the foreground and sea clutter as the background. Background is relatively fixed among the produced spectrum sequence, which means that they are highly correlated among different frames, forming a low-rank matrix B. The constraint on B can be expressed as

$$rank(B) \le K \tag{11}$$

where K is a constant that is predefined, and reflects the complexity of the background model.

Simultaneously, the foreground areas are defined as radar targets that move differently from the background, and the targets act as outliers in the low-rank representation. The binary states of entries in the foreground support S can be modeled by a Markov random field [43]. Consider a graph $G = (\nu, \varepsilon)$, where ν is the set of vertices denoting all $Q \times N$ pixels in the sequence and ε is the set of edges connecting spatially or temporally neighboring pixels. Let h be the size of the edge set and $y = Q \times N$ be the size of the vertex set. The node-edge incidence matrix of G is a $h \times y$ matrix, and the $(i, j)^{th}$ entry of the incidence matrix A is defined as follows:

$$A(i,j) = \begin{cases} 1\,, & \text{if } v_j \text{ equals one of the endpoints of } \varepsilon_i \\ 0\,, & \text{if } v_j \text{ does not equal one of the endpoints of } \varepsilon_i \end{cases} \tag{12}$$

Assuming that we have no additional prior knowledge about the locations of objects, the energy of S is given by the Ising model [43] as

$$\beta \sum_{qn\in\nu} S_{qn} + \gamma \sum_{(qn,pm)\in\varepsilon} |S_{qn} - S_{pm}| \tag{13}$$

where $\beta > 0$ represents the potential of S_{qn} being 0 or 1, and $\gamma > 0$ controls the strength of dependence between S_{qn} and S_{pm}. Finally, we consider the signal model that describes the formation of X. On the one hand, in the foreground, $S_{qn} = 1$, X_{qn} equals to the foreground intensity, and X_{qn} is not constrained. On the other hand, in the background, $S_{qn} = 0$ and $X_{qn} = B_{qn} + \mu_{qn}$, where μ_{qn} denotes independent and identically distributed Gaussian noise. Thus, B_{qn} should provide the best fit of X_{qn} in the least squares sense in this case.

By combining the above background, foreground and signal models, the objective function for estimating B and S is given by

$$\begin{aligned} \min_{B,S_{qn}\in\{0,1\}} & \frac{1}{2} \sum_{qn:S_{qn}=0} (X_{qn} - B_{qn})^2 \\ & + \beta \sum_{qn\in\nu} S_{qn} + \gamma \sum_{(qn,pm)\in\varepsilon} |S_{qn} - S_{pm}| \\ s.t.\ & rank(B) < K \end{aligned} \tag{14}$$

To make (14) tractable, the rank operator associated with B is relaxed with the kernel norm [44]. By rewriting (14) in the dual form and with matrix operators, we obtain the following problem:

$$\begin{aligned} \min_{B,S_{qn}\in\{0,1\}} & \frac{1}{2} \left\| p_{S^\perp}(X - B) \right\|_F^2 + \alpha \|B\|_* + \beta \|S\|_1 \\ & + \gamma \|A \cdot vec(S)\|_1 \end{aligned} \tag{15}$$

where $|\cdot|$F is the Frobenius norm, $|\cdot|^*\cdot$ is the nuclear norm, and $|\cdot|_1\cdot$ is the ℓ_1 norm. A is the node-edge incidence matrix of G, and vec represents the vectorization of matrix S. The parameter $\alpha > 0$ is related to the low-rank background K. The parameters α, β, and γ represent the weights of the low-rank background, sparse foreground, and smooth foreground. To minimize the function, these parameters should be adjusted properly.

3) ALGORITHM

The objective function defined in (15) is nonconvex and it includes both continuous and discrete variables. We adopt an alternating algorithm that separates the energy minimization over B and S into two steps. To estimate the support $\hat{S}$, the minimization in (15) over B turns out to be the matrix completion problem [45]:

$$\min_{B} \frac{1}{2} \left\| p_{\hat{S}^\perp}(X - B) \right\|_F^2 + \alpha \|B\|_* \tag{16}$$

The optimal B can be computed efficiently by the SOFT-IMPUTE algorithm [45], which makes use of the following lemma [46]:

Lemma 1: Given a matrix Z, the solution to the optimization problem

$$\min_{I} \frac{1}{2} \|Z - I\|_F^2 + \omega \|I\|_* \tag{17}$$

is given by $\hat{I} = \Theta_\omega(Z)$, where Θ_ω is the singular value threshold

$$\Theta_\omega(Z) = U \sum\nolimits_{\omega} V^{\mathrm{T}} \tag{18}$$

where $\sum_\omega = \mathrm{diag}[(d_1 - \omega)_+, \ldots, (d_\mathrm{r} - \omega)_+]$, $U \sum V^T$ is the *SVD* of Z, $\sum = \mathrm{diag}[d_1, \ldots, d_\mathrm{r}]$, and $\xi_+ = \max(\xi, 0)$.

With Lemma 1, the optimal solution can be obtained by iteratively using

$$\hat{B} \leftarrow \Theta_\alpha(p_{\hat{S}^\perp}(X) + p_{\hat{S}}(\hat{B})) \tag{19}$$

with arbitrarily initialized B.

To minimize the energy in (15) over S given the low-rank matrix and the energy can be described as

$$\begin{aligned} &\frac{1}{2} \left\| \mathrm{p}_{\mathrm{S}^\perp}(X - \hat{B}) \right\|_F^2 + \beta \|S\|_1 + \gamma \|A \cdot vec(S)\|_1 \\ &\quad = \sum_{i,j} (\beta - \frac{1}{2}(X_{ij} - \hat{B}_{ij})^2) S_{ij} + \gamma \|A \cdot vec(S)\|_1 \\ &\qquad + \frac{1}{2} \sum\nolimits_{ij} (X_{ij} - \hat{B}_{ij})^2 \end{aligned} \tag{20}$$

The above mentioned energy is in the standard form of the first-order MRFs with binary labels, which can be solved exactly using graph cuts [47], [48].

For details about the estimation, we refer to [40] about the selection of the parameters α, β, and γ. Specifically, α is initialized to be the second largest singular value of X and is reduced by a factor $\eta_1 = 1/\sqrt{2}$ until $\mathrm{rank}(B) > K$. A similar procedure is followed for β, starting at a relatively large value and then decreasing by a factor of $\eta_2 = 1/2$ after each iteration until β reaches $4.5\hat{\sigma}^2$, where $\hat{\sigma}^2$ is the estimated noise level calculated from the variance of $X - B$. Overall, only two parameters, K and γ, need to be selected. The optimization algorithm is empirically configured by setting $K = \left\lfloor \sqrt{N} \right\rfloor$ and $\gamma = 5\beta$, where $\lfloor\rfloor$ means the lower integer part.

All the steps involved in solving the optimal model with adaptive parameter tuning are summarized in Algorithm 1.

Algorithm 1 Separating Targets and Sea Clutter by the Low-Rank Method

1. **Input** : $X = [x_1, x_2, \ldots, x_\mathrm{N}]$
2. **Initialize** : $\hat{B} \leftarrow X$, $\hat{S} \leftarrow \mathbf{0}$, α, β.
3. **Output** : $\hat{B}$, $\hat{S}$
4. **Repeat**
5. $\hat{B} \leftarrow \Theta_\alpha(p_{\hat{S}^\perp}(X) + p_{\hat{S}}(\hat{B}))$;
6. **until** convergence
7. **if** $rank(\hat{B}) \leq K$ **then**
8. $\alpha \leftarrow \eta_1 \alpha$;
9. **go to** step3;
10. **end if**
11. estimate $\hat{\sigma}$;
12. $\hat{\beta} \leftarrow \max(\eta_2 \beta,\ 4.5\hat{\sigma}^2)$;
13. $\hat{S} \leftarrow \arg\min_S \sum_{ij} (\beta - \frac{1}{2}(I_{ij} - \hat{B}_{ij})^2) S_{ij} + \gamma \|A\ vec(S)\|_1$
14. **until** convergence

B. CLUTTER REMOVAL FOR TARGET DETECTION

The low-rank representation mentioned in section A is used to separate the target (foreground) from the sea clutter (background), which can suppress the sea clutter of radar to improve the signal-to-clutter ratio (*SCR*). However, considering the influence of wind, wave and current, the sea surface is time-varying within a certain range, causing part of the background to be separated into the foreground. In this case, clutter and slow targets are difficult to distinguish because they are all around zero Doppler values. In this section, a sea clutter discriminator is constructed by defining the background frequency to further remove the clutter in the foreground, so as to suppress false alarm and improve detection rate.

1) CLUTTER REMOVAL VIA THE CLUTTER DISCRIMINATOR

Assuming that the foreground frequency and background frequency are defined as the sum of the foreground and background frame sequences, respectively, which are denoted as F_S and F_B

$$F_S(r, d) = \sum_{i=1}^{N} S_i(r, d) X_i(r, d) \tag{21}$$

$$F_B(r, d) = \sum_{i=1}^{N} B_i(r, d) \tag{22}$$

where $r = 1 \ldots R_0$ and $d = 1 \ldots D_0$ represent the range bin and Doppler bin, respectively. For pixels in the foreground

frequency, the larger the value, the more likely it is to be a target. Similarly to the background frequency, the larger value means a greater probability that the pixel is sea clutter. Therefore, within the Doppler bandwidth of sea clutter, for any pixel point $g \in F_{\mathrm{B}}$, if $g \geq f_{\mathrm{T}}$, g represents sea clutter; otherwise, g does not represent sea clutter, where f_{T} is the predefined threshold

$$g = \begin{cases} 1, & g \geq f_T \\ 0, & g < f_T, \end{cases} \quad g \in F_B \tag{23}$$

By traversing all the pixels of the background frequency according to (23), the sea clutter discriminator of the range-Doppler spectrum sequence can be obtained as M_{d}. The key to obtain the discriminator is the value of f_{T}, if the value of f_{T} is too large, the amount of clutter considered by the sea clutter discriminator will be too small, which can lead to false alarms; conversely, if the value of f_{T} is too small, the amount of clutter considered by the sea clutter discriminator will be too large, which can lead to missed detections. Therefore, the value of f_{T} directly affects the detection performance, and the specific parameter selection process will be discussed in section III C.

The sea clutter discriminator is used to eliminate the sea clutter in the foreground frequency, and the result is expressed as F_{opt}

$$F_{\mathrm{opt}} = F_S(r, d) - F_S(r, d) \cdot M_d \tag{24}$$

$\forall l \in F_{opt}$, if $(F_{\mathrm{opt}})_{r,d} > 0$, the pixel l represents a target; otherwise, l does not represent a target. Hence, the moving targets in each frame are shown as

$$Y_i = S_i F_{\mathrm{opt}}, \quad i = 1 \ldots N \tag{25}$$

where Y_{i} is the ith foreground after clutter elimination.

2) RELOCATION AND VELOCITY INVERSION OF TARGET

Since a moving target has a radial velocity, the moving target will have an "extra" frequency shift to deviate from its real position in the range-Doppler spectrum; hence, the detected moving target needs to be repositioned. In this section, based on dual channel radar, targets are repositioned with the phase-comparison method [49]. By using the center azimuth of radar beam θ_0 and the beam width $\Delta\theta$, the azimuth of the moving target is expressed as $\theta_0 + \Delta\theta'(-\Delta\theta/2 \leq \Delta\theta' \leq \Delta\theta/2)$. Assuming that the target signals received by the sum channel and difference channel of radar are e_1 and e_2, respectively, the coherent phase difference is $e_{12} = e_1 \cdot e_2^*$. Thus, $\Delta\theta'$ is

$$\Delta\theta' = \frac{\lambda \arg[e_{12}]}{2\pi d_0 \sin\theta_0 \cos\varphi} \tag{26}$$

where d_0 is the length of radar baseline. The true azimuth of the target is obtained as $\theta_0 + \Delta\theta'$. Combined with the aircraft inertial navigation information and the position information of the target in the range-Doppler spectrum, the target is accurately located in the actual scene.

The radial velocity v_{r} of the target is retrieved by using the Doppler frequency f_{d} of the target

$$v_{\mathrm{r}} = \frac{\lambda f_d}{2} \tag{27}$$

After the velocity of the target is obtained, the target is tracked based on the position, velocity and time information.

III. APPLICATION TO AIRBORNE MARITIME SURVEILLANCE RADAR

The method developed based on the low rank representation is applied to the measured airborne radar data, and the feasibility of this method is verified at different azimuth angles. First, the acquisition of experimental data is introduced. Then, the sea clutter characteristics of airborne radar data are analyzed, and the necessity of separating sea clutter from a target is illustrated. Finally, the sea clutter discriminator is used to further remove the clutter in the foreground, and the positions and tracks of targets are obtained.

A. EXPERIMENTAL DATA

Experimental data were collected from the sea area near Guangdong, and the latitude and longitude range of the experimental area is shown in the red box in Fig. 4.

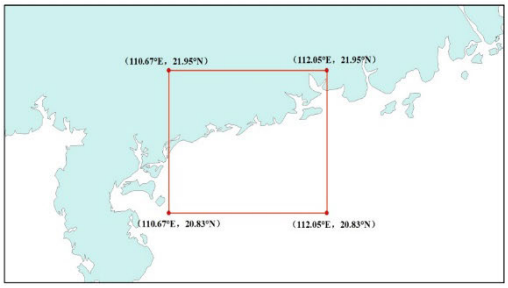

FIGURE 4. The location of the experimental area. The range of the latitude and longitude is shown in the red box.

The 3D geometry of the airborne maritime surveillance radar is shown in Fig. 2. The radar antenna provided continuous periodic scanning during the flight, and the inertial navigation system was used to record the flight attitude, thus achieving sector scanning within the range of $[-120°-120°]$. The settings of the radar parameters are shown in Table 1. The pitch angle of the radar beam center was 84.7°, which reflects a small grazing angle observation.

Furthermore, synchronized automatic identification system (AIS) data were obtained in the experiment to provide a reference for the analysis of the ship detection performance. As shown in Fig. 5, a total of 1716 ships were obtained through AIS data analysis, among which, fishing boats accounted for approximately half of all boats, followed by cargos ships and tankers; more than half of the ships were less than 50 m and 10 m in length and width, respectively.

TABLE 1. The parameters of the airborne maritime surveillance radar.

Name	Value
Flight height (m)	3000
Flight velocity (m/s)	40-50
Carrier frequency (GHz)	10
Pulse repetition frequency (Hz)	2500
Band width (MHz)	9
Range resolution (m)	7.5
Number of radar channels	2
Elevation angle (°)	84.7
Scanning cycle (s)	16
Scanned area (°)	-120-120
Sample number (range)	4096
Sample number (azimuth)	128

B. LOW-RANK APPROACH APPLIED TO SEA CLUTTER SUPPRESSION

For clutter suppression, the necessity of separating sea clutter and targets is analyzed. Then, the performance of the proposed method in sea clutter suppression is compared with that of space-time adaptive processing (STAP) and principal component pursuit (PCP), and the results indicate that the sea clutter suppression performance of low-rank representation is optimal. Moreover, the selection of parameters is analyzed.

1) SEA CLUTTER ANALYSIS

Suppose that a plane flies in a certain direction, considering that the flight distance of the plane between adjacent periods is far less than the slant distance; therefore, for the same location, the variation in the radar azimuth angle of adjacent periods is very small. In this case, the sequences can be formed by the range-Doppler spectra at the same radar azimuth. X_θ is defined as the range-Doppler spectrum sequence corresponding to the radar azimuth angle θ. The sampling number of the Doppler frequency corresponds to 128, and that value is adopted in this paper.

The data shown in Fig. 6(a) is the $N/2$ frame of a range-Doppler spectrum sequence with $N = 40$ and $\theta = 4.2°$ that was collected from 10:30 to 10:35 on November 24, 2018. Sea clutter is mainly located in the vicinity of the zero Doppler frequency, which is related to the slow changes in sea clutter, forming a small Doppler frequency shift. The red boxes in Fig. 6(a) contain three targets with $r_1 = 293$, $r_2 = 2493$ and $r_3 = 3913$. Target 3 is outside the sea clutter bandwidth, while target 1 and target 2 are located near the zero Doppler spectrum, which is difficult to separate from sea clutter. Fig. 6 (b) compares the power of the targets and sea clutter. The solid lines represent the power of targets, the dashed lines represent the average power of sea clutter around the target, and sea clutter 1-3 corresponds to the targets 1-3, respectively. The peak power of target 1 is 2.2dB higher than the average power of sea clutter, and the differences in the powers of targets 2 and 3 are 2.21dB and 9.16dB, respectively. This result indicates that the power of target 3 is significantly greater than that of the surrounding sea clutter, and can be detected easily, while targets 1 and 2 are submerged in the sea clutter, which makes them difficult for traditional methods to detect.

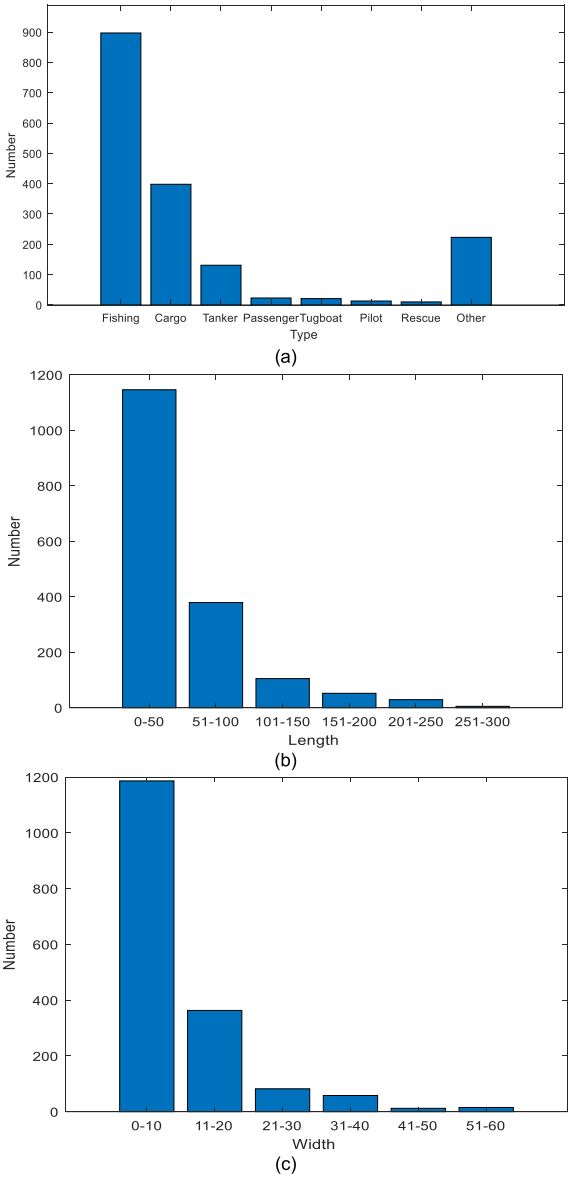

FIGURE 5. Type, length and width information of ships extracted from AIS data. (a) Statistical distribution of the ship type. (b) Statistical distribution of the ship length. (c) Statistical distribution of the ship width.

2) PERFORMANCE OF SEA CLUTTER SUPPRESSION

Based on the range-Doppler spectrum sequence generated at the corresponding azimuth angle, the effectiveness of the low-rank representation method for separating targets and sea clutter is demonstrated. Taking $\theta = 1.85°$ as an example, the range-Doppler spectrum sequence is expressed as X_θ. Fig. 7 shows the result of the $N/2$ frame with $N = 32$; (a)-(c) are the input range-Doppler data, background (sea clutter) and foreground (target), respectively. In comparison with the input range-Doppler data, the shape of the sea clutter spectrum in the background is obvious, and the non-clutter

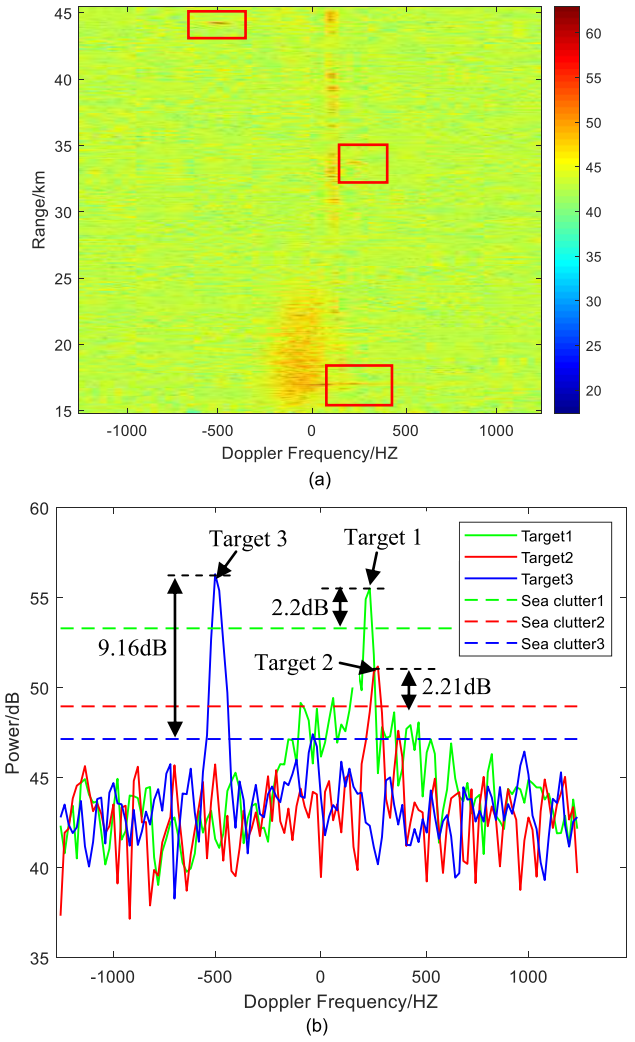

FIGURE 6. Sea clutter analysis of airborne maritime surveillance radar with $\theta = 4.2°$, $N/2$ frame, and $N = 40$. (a) The power of the $N/2$ frame of the range-Doppler spectrum. (b) The power comparison of targets and sea clutter.

area is very clean; moving targets are all separated into the foreground. Note that some sea clutter exists around the zero Doppler frequency in the foreground, which is due to the dynamic changes of the sea surface, as previously mentioned. This clutter will be further removed in section C.

Experiments were performed using real radar data to validate the superiority of the proposed method in clutter suppression. The low-rank method was compared with STAP and PCP. STAP [24], [50] is a classical clutter suppression method that combines spatial and temporal dimensions for filtering. Similar to the proposed method, targets and sea clutter are separated by sparse and low-rank matrix decomposition in PCP [4], [39]. The proposed method models the foreground using Markov Random Field, and the accuracy of detecting contiguous outliers is better than PCP (without considering Markov property). PCP uses the convex relaxation by replacing rank (B) with $|B|_*$ and $|S|_0$ with $|S|_1$, while the proposed method only relaxes the rank penalty and keeps the l_0-penalty on S to preserve the robustness to outliers. Therefore, the proposed method is more applicable than PCP to target detection for airborne radar in scanning mode.

The results of the STAP (1DT-STAP, 3DT-STAP and sparse-STAP), PCP and low-rank methods are shown in Fig. 8, (a) represents the raw range-Doppler data in dB (the $N/2$ frame with $N = 32$); (b)-(d) represent the results of 1DT-STAP, 3DT-STAP and sparse-STAP, respectively; (e) illustrates the result of the PCP method; (f) represents the result of the low-rank representation method. These methods all suppressed sea clutter to some degree and improved the SCR, making them useful for the detection of ship targets. Among these methods, the sea clutter suppression performance based on the low-rank representation method is obviously better than that of other methods. Two targets (range cells 284 and 3912) are marked with red boxes. Fig. 9(a)-(b) shows the performance of the five methods for range cells 284 and 3912; notably, the power of clutter decreases in all five methods. However, for the STAP and PCP methods, the power of both sea clutter and ship targets decreases, resulting in the power loss of targets. The sea clutter suppression method based on the low-rank representation developed in this paper can reduce the sea clutter power while maintaining the target power, thus significantly improving the contrast between ship targets and sea clutter, and enhancing the detection ability of ship targets.

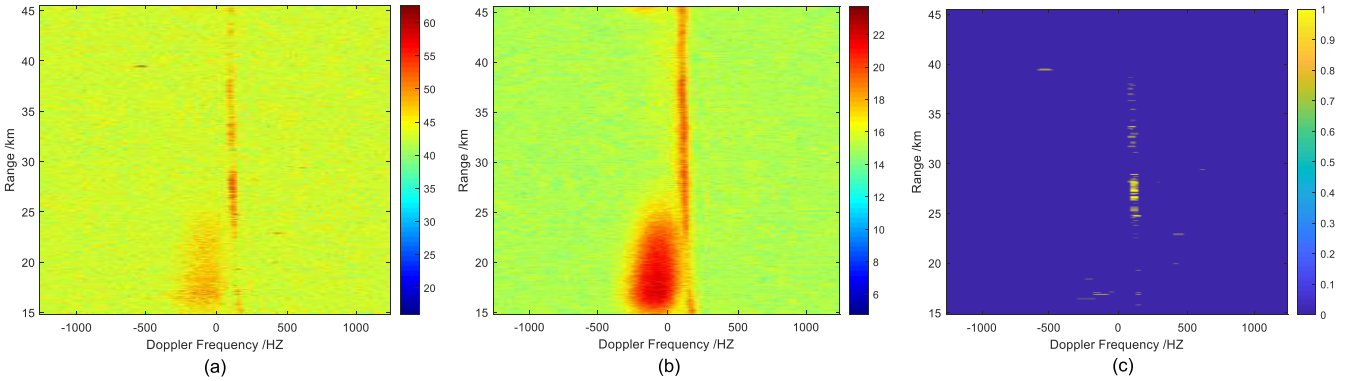

FIGURE 7. Background and foreground extraction based on the low-rank representation. (a) Raw spectrum $X_{N/2}$ in dB. (b) Low-rank background $B_{N/2}$. (c) Foreground $S_{N/2}$.

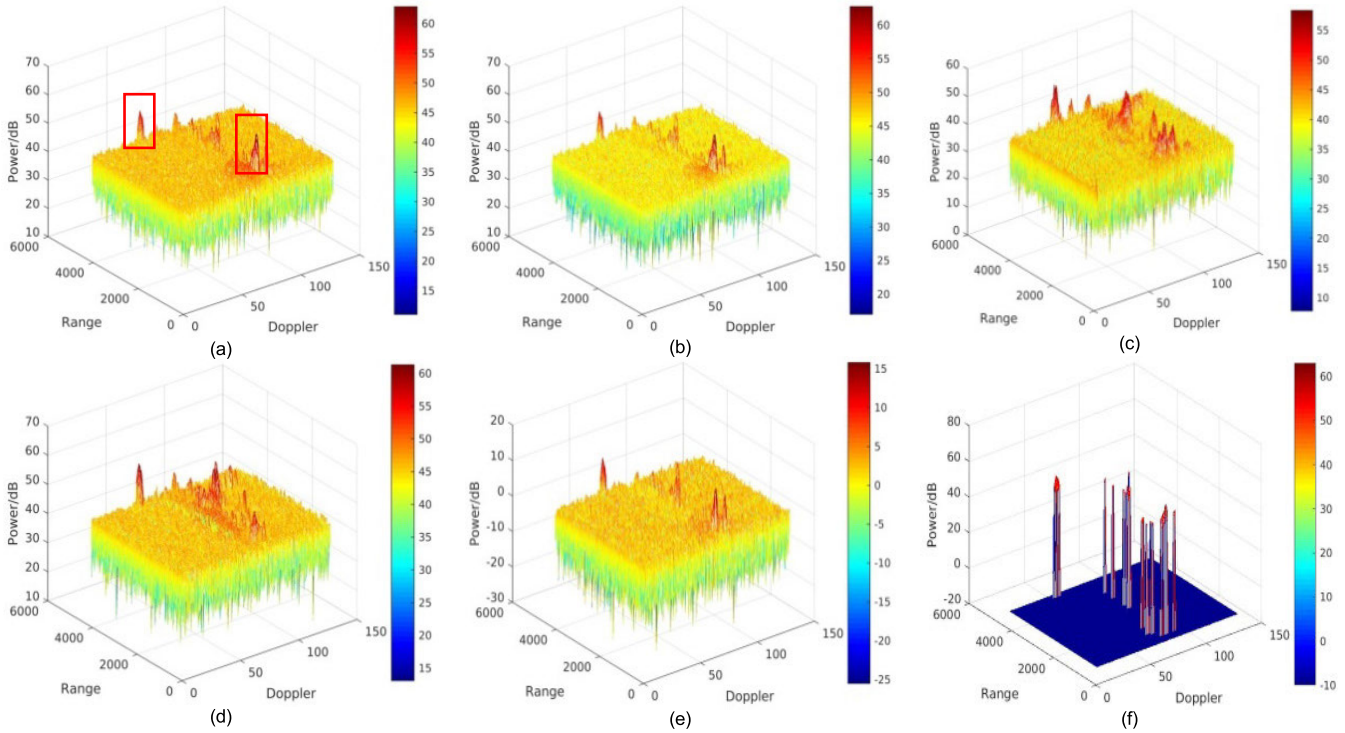

FIGURE 8. Clutter suppression results of the five methods, the $N/2$ frame, $N = 32$. (a) Raw range-Doppler data in dB. (b) 1DT-STAP. (c) 3DT-STAP. (d) Sparse-STAP. (e) PCP. (f) Proposed low-rank representation method.

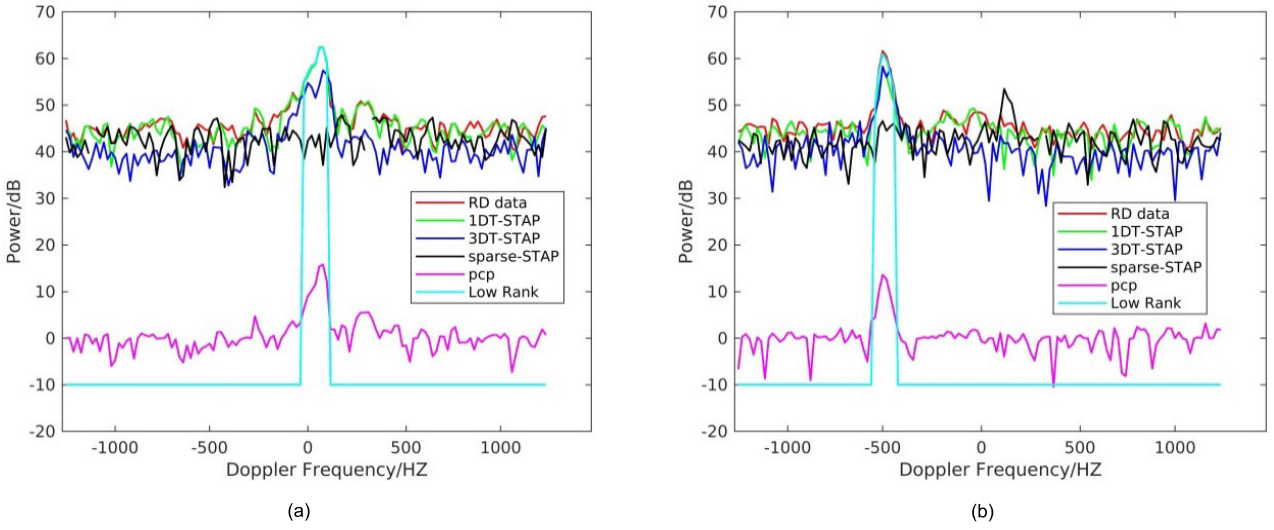

FIGURE 9. Performance of clutter suppression with range cells 284 and 3912 in Figure 8. (a) Performance of clutter suppression with range cell 284. (b) Performance of clutter suppression with range cell 3912.

To quantitatively evaluate the performance of the 1DT-STAP, 3DT-STAP, sparse-STAP, PCP and proposed low-rank representation methods, targets and the surrounding sea clutter samples are selected to calculate the sample mean values and *SCR*. The *SCR* values for 5 random targets are listed in Table 2. All five methods improved the *SCR*, making it easier to distinguish ship targets from sea clutter. In detail, the low-rank matrix representation method displays the best performance, and the corresponding *SCR* is 4 times more than that before clutter suppression. The performance of the other methods decreased in the following order: sparse-STAP, 3DT-STAP, PCP and 1DT-STAP. The sparse-STAP method is mostly used for sea clutter suppression with multichannel radar data. In this paper, the radar data are based on only two channels, which may limit its performance. Compared with 1DT-STAP, 3DT-STAP achieves the

TABLE 2. The SCRs of five targets based on five clutter suppression methods.

Methods	Target 1	Target 2	Target 3	Target 4	Target 5
Raw data	12.47	9.04	14.24	5.03	5.78
1DT	14.05	10.14	16	8.72	9.25
3DT	18.27	19.17	17.97	10.88	13.11
sparse	15.26	19.19	25.05	14.9	17.59
PCP	15.98	14.32	18.12	13.52	15.08
Low-rank	65.46	42.32	57.43	42.46	46.52

suppression of sea clutter in the two-dimensional plane of time and space.

For the same kind of separation method PCP and the proposed low-rank method, the Euclidean distance and Chebyshev distance are introduced to represent the degree of separation between target and sea clutter. The Euclidean distance [51] is defined as

$$ED = \frac{|M_{\text{ship}} - M_{\text{sea}}|}{\sqrt{\sigma^2_{\text{ship}} + \sigma^2_{\text{sea}}}} \tag{28}$$

where M_{ship} and M_{sea} correspond to the statistical average of the samples of ships and the sea surface, and σ^2_{ship} and σ^2_{sea} denote the variance of the samples of ships and sea surface, respectively. This equation implies that the larger the distance is, the better the performance in distinguishing ships from the surrounding sea.

The Chebyshev distance [52] is defined as

$$CD = \max(x_{\text{ship}} - x_{\text{sea}}) \tag{29}$$

where x_{ship} and x_{sea} correspond to the sample value of ships and the sea surface, respectively. The larger the distance, the better performance in separating targets and sea clutter. The results of PCP and the proposed low-rank method are shown in Table 3, the Euclidean distance and Chebyshev distance between five targets and sea clutter are listed, and the Euclidean distance and Chebyshev distance of the proposed low-rank method are all more than two times of PCP method, which implies that the proposed low-rank method is better in sea clutter suppression than PCP method and is of great benefit to ship detection.

TABLE 3. The distance of five targets based on PCP and the proposed low-rank methods.

Distance	Method	Target 1	Target 2	Target 3	Target 4	Target 5
ED	Raw data	5.73	3.23	4.94	1.95	2.04
	PCP	6.56	5.38	6.49	5.4	5.61
	Low-rank	31.04	11.43	16.72	11.43	12.18
CD	Raw data	16.85	15.27	24.79	16.13	19.9
	PCP	19.72	19.86	29.97	27.88	26
	Low-rank	68.99	52.33	64.9	63.51	58.3

3) PARAMETER SELECTION

The influence of length N and interval L of the range-Doppler sequence on the *SCNR* is discussed in this section. As shown in Fig. 10(a), the sequence length ranges from 3 to 30 with interval 3. The *SCNR* is almost constant with the increasing sequence length. Apart from target 3 in Fig. 10(b), the result of the sequence interval L is consistent with variations in the length N, and the value of target 3 with interval 32 may be related to the selection of samples. In general, the influence of the sequence length and sequence interval on the *SCNR* is negligible, indicating the robustness of the proposed method.

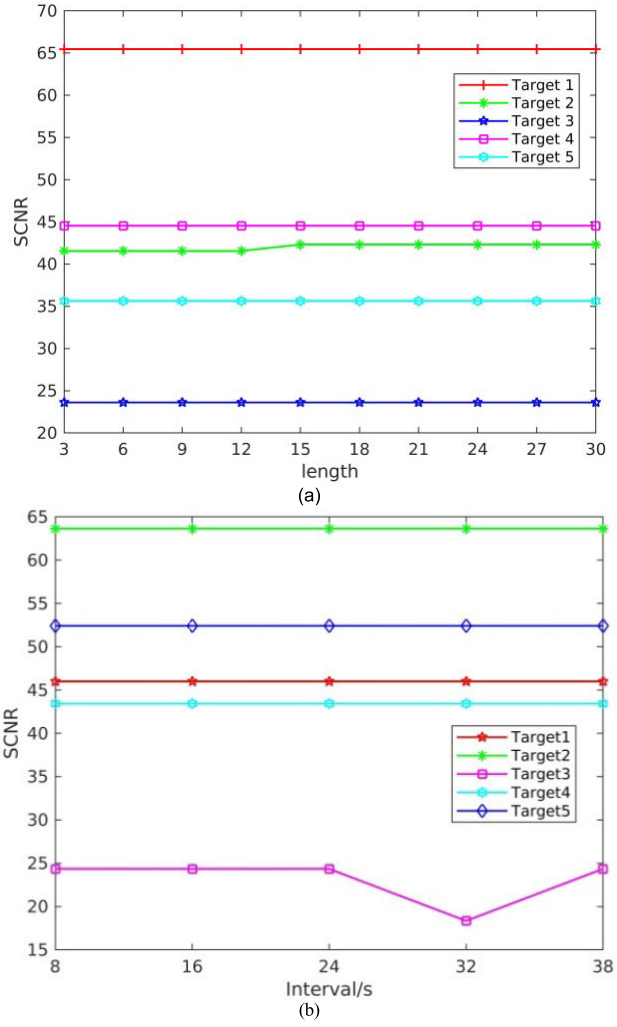

FIGURE 10. Effect of the parameter selection (N and L) on *SCNR*. (a) Sequence length *N*; (b) Sequence interval *L*.

C. APPLICATION TO TARGET DETECTION

Because some sea clutter is separated into the foreground, the sea clutter discriminator is constructed by defining the foreground frequency and background frequency to further remove the sea clutter, and improve the detection rate of ship targets. The background frequency and foreground frequency defined in section II are listed in Fig. 11(a)-(b) with

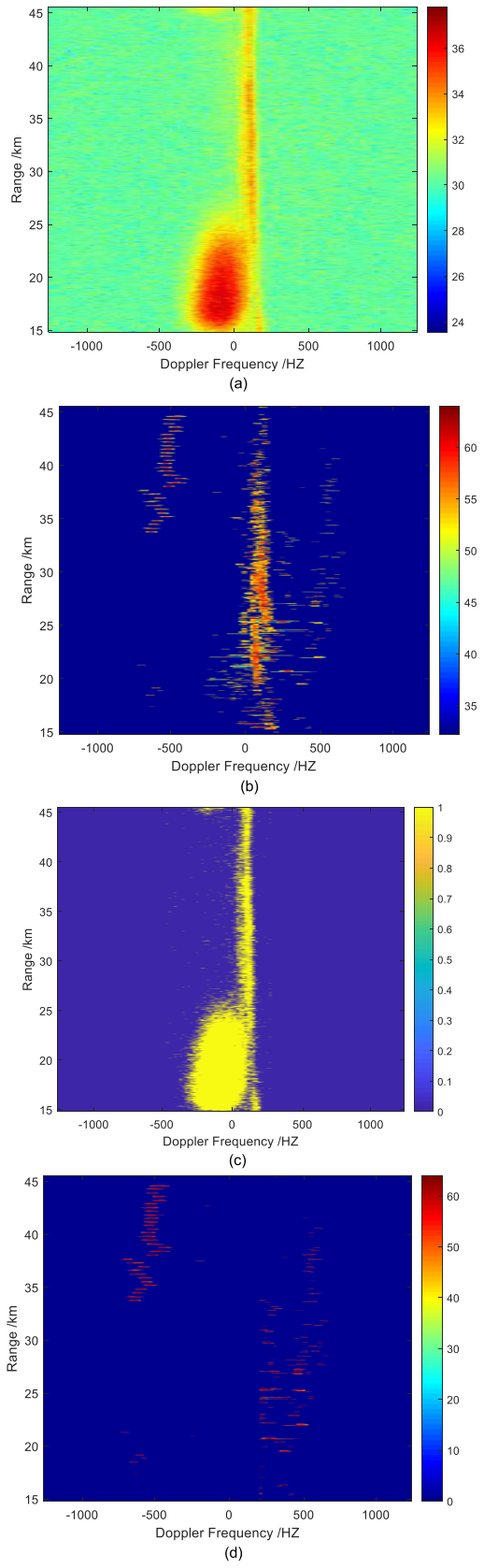

FIGURE 11. Ship detection results based on the low-rank representation method with $\theta = 1.85°$. (a) Background frequency. (b) Foreground frequency. (c) Sea clutter discriminator. (d) Result of clutter removal.

$\theta = 1.85°$. The sea clutter is located near the zero Doppler frequency and has a clear profile shown in (a); the ship targets in (b) are clear, and the suspected tracks along the range are formed.

However, sea clutter in the foreground is still serious and ought to be removed for slow target detection. The sea clutter discriminator in Fig. 11(c) is obtained by selecting the appropriate threshold to segment the background frequency (a) within the sea clutter bandwidth, and the experience threshold is set to $1.5M$, where M is the mean of the background frequency. Yellow pixels represent sea clutter with values of 1, and blue pixels represent non-clutter points with values of 0. According to (24), the result of sea clutter removal is obtained as (d) by using (b) and (c). Notably, the sea clutter around the zero Doppler frequency is significantly reduced, that is to say, false alarms are avoided without reducing the target power, which facilitates the detection of slow ship targets and provides a foundation for the generation of tracks.

Comparisons of the low-rank, PCP and CFAR detectors were made to verify the superiority of the low-rank method for ship detection. For PCP method, the values of targets are greater than 0, while the values of sea clutter are less than 0 with large amount of experiments. Hence, 0 can be used to separate targets and sea clutter. Among these methods, a threshold of 0 is adopted to detect targets after clutter suppression in the PCP method, and the CFAR method is based on sparse-STAP with a false alarm rate of 0.001. Considering the false alarm rate and detection rate, the *FOM* is used for detection performance analysis [53]:

$$FOM = \frac{N_{tt}}{N_{fa} + N_{gt}} \tag{30}$$

where N_{tt} and N_{fa} are the numbers of detected ships and false alarms, respectively. N_{gt} is the number of ships that matched with AIS. The larger the *FOM* is, the better the detection performance. Five range-Doppler sequences extracted from five experiments are utilized to evaluate the ship detection performance of different methods, and the corresponding azimuth angles are expressed as θ_1-θ_5, where $\theta_1 = 1.85°$, $\theta_2 = -118.57°$, $\theta_3 = 4.20°$, $\theta_4 = -57.42°$ and $\theta_5 = 89.33°$. Combined with AIS, the numbers of ships corresponding to θ_1-θ_5 are 227, 95, 284, 191 and 202, respectively. The results of the CFAR, PCP and low-rank methods are listed in Table 4. The *FOMs* of the CFAR, PCP and low-rank methods are 0.8, 0.85 and 0.97, respectively, according to (30). The results demonstrate that the low-rank method performs best, followed by PCP, and the CFAR method performs worst.

TABLE 4. Detection results of the CFAR, PCP and low-rank methods.

Method	Correct Detections	False Alarms	*FOM*
CFAR	253	31	0.8
PCP	249	9	0.85
Low-rank	282	5	0.97

TABLE 5. Detailed information for the matched ships.

No.	MMSI	Name	Type	(Length,width)	Time_UTC	Mean velocity (knot)
1	160400725	HHH	Fishing	(49,8)	2018.11.24 2:39:19-2:49:54	7.47
2	412468254	YUEDIANYU46998	Fishing	(32,6)	2018.11.21 3:54:37-4:22:13	8.65
3	413481450	YUEANYUN67	Cargo	(98,16)	2018.11.21 3:06:18-3:37:18	5.83
4	412478356	YUE YANG JIANG06179	Fishing	(29,6)	2018.11.24 2:59:52-3:14:52	7.4
5	412476346	YUEYANGDONGY U13 78	Fishing	(31,6)	2018.11.21 3:47:22-4:03:25	7.1
6	412470892	YUEYANGDONGY U13238	Fishing	(38,6)	2018.11.21 3:48:55-4:02:06	7.47
7	413488260	YUN DA YOU 6	Tanker	(85,12)	2018/11/21 9:49:15-10:06:34	8.26
8	413438060	HENG FAN 18	Tanker	(53,9)	2018/11/21 9:49:1-10:05:21	8.25
9	138999998		passenger ship	(29,6)	2018/11/21 9:48:50-10:9:49	2.8

The impact of threshold selection on ship target detection in sea clutter discriminator generation is analyzed below. By using the five range-Doppler sequences extracted from five experiments, Fig. 12 (a)-(b) show the changes in the false alarm rate (Pfa) and detection rate (Pd) as the threshold increases, and the threshold ranges from $0.75M$ to $3M$. The curves 1-5 correspond to the azimuth θ_1-θ_5. Overall, the detection rate and false alarm rate increase as the threshold increases, and the trend is the same. If the threshold is greater than $1.5M$, the false alarm rate increases rapidly, while the detection rate tends to 1. To reduce the false alarm rate while maintaining an appropriate detection rate, the optimal threshold in this paper is set to be $1.5M$, where M is the mean of the background frequency.

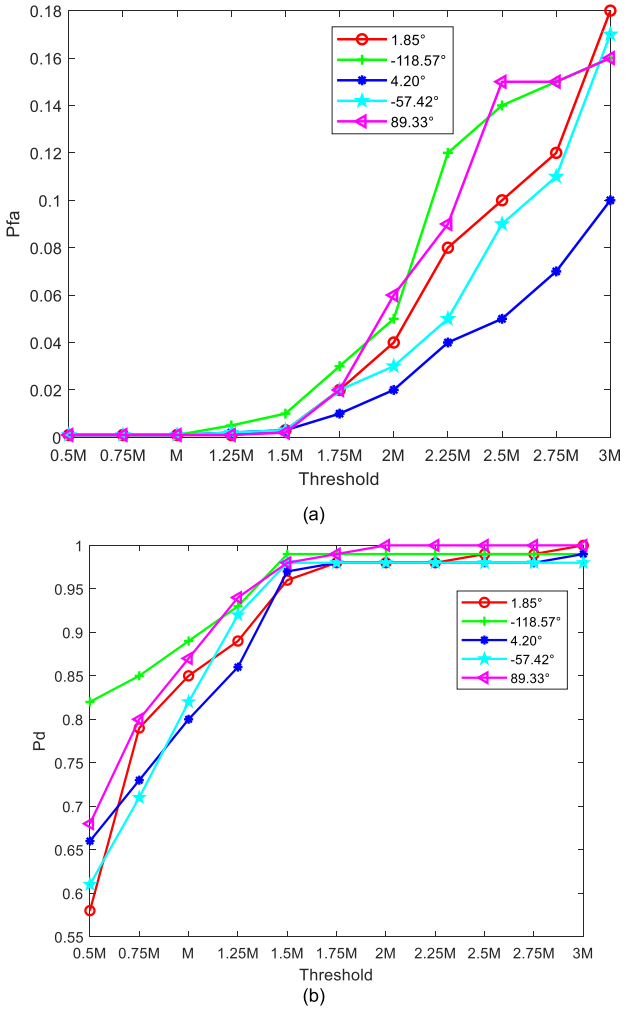

FIGURE 12. The impact of threshold selection on the false alarm rate and detection rate, where *M* is the mean of the background frequency. (a) The variation in the false alarm rate with various thresholds. (b) The variation in the detection rate with various thresholds.

D. APPLICATION FOR TARGET TRACKING

On the basis of clutter suppression and ship detection, the location and velocity of ships can be obtained after the processes of relocation and velocity inversion, respectively. Subsequently the tracks of ships are obtained via location and time updates. Matching with the AIS information according to the time and location, the tracks of targets are shown in Fig. 13, in which red represents the ships detected by the low-rank method and green represents the ships obtained from the AIS. The time difference and location difference are set to 0 s and 1 km, respectively. The x-coordinate of Fig. 13 is longitude, and the y-coordinate is latitude. The six tracks demonstrate the effectiveness of the low-rank method in ship detection and tracking. The detailed information for ships in Fig. 13 is listed in Table 5.

Fig. 14 shows the relationship between the inversion velocity and the AIS velocity of ships. The abscissa represents the inversion velocity of the target, and the ordinate represents the AIS velocity of the target. The velocity of the ships is mainly distributed near the 45° line, which reflects strong consistency between the inversion velocity and AIS velocity, indicating that the inversion accuracy of the target velocity is high. The mean error of velocity inversion is 0.12 m/s and the mean relative error is 4.7%.

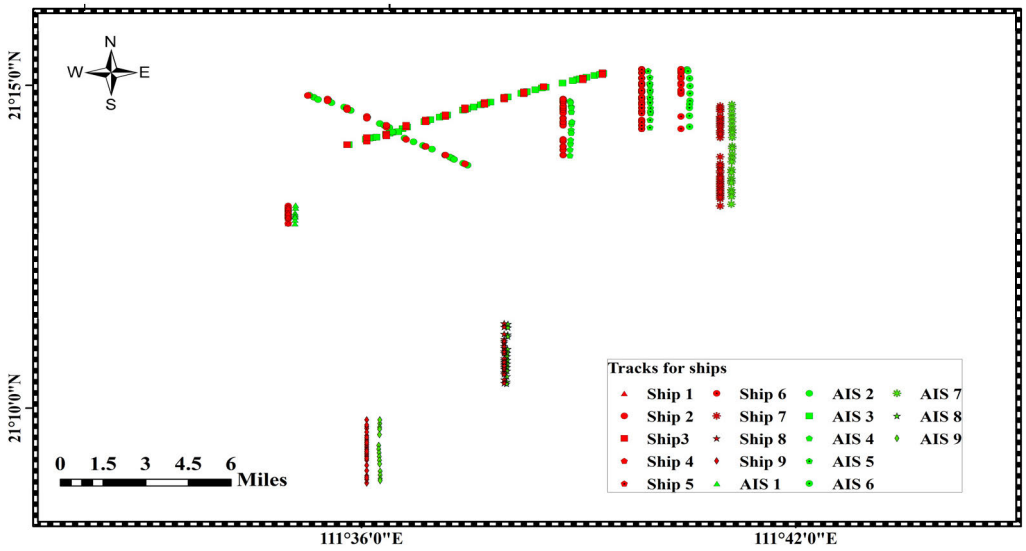

FIGURE 13. Tracks of ships obtained from the detection results and AIS information.

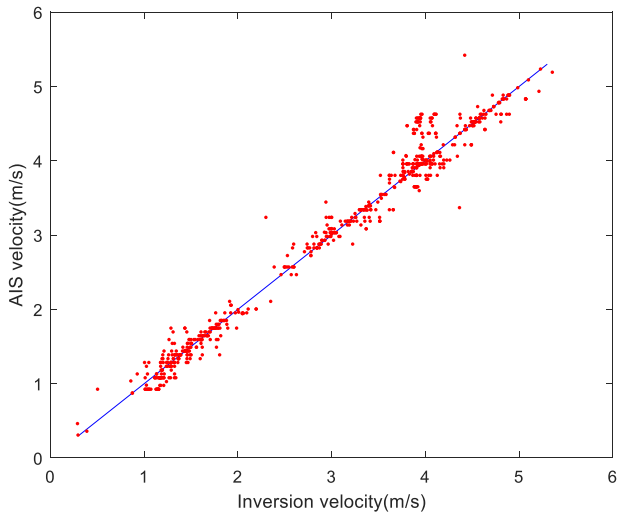

FIGURE 14. The relation between inversion velocity and AIS velocity of ships.

IV. CONCLUSION

The focus of this paper is on clutter suppression and target tracking for maritime surveillance radar. A new method is proposed to separate radar targets from the surrounding sea clutter in a low-rank representation. Experiments demonstrated that the low-rank method is obviously superior to 1DT-STAP, 3DT-STAP, sparse-STAP and PCP in clutter suppression without reducing the power of targets. Specifically, the low-rank matrix method displayed the best performance, and the corresponding SCR was 4 times better than that before clutter suppression. The performance of the other methods decreased in the following order: sparse-STAP, 3DT-STAP, PCP and 1DT-STAP. To further remove the sea clutter caused by sea surface motion in the foreground, a sea clutter discriminator is constructed within the sea clutter bandwidth. The recommended threshold for clutter discriminator generation was set to be $1.5M$ based on experimental analysis, where M is the mean of the background frequency. Comparisons of CFAR, PCP and the low-rank methods were made, and the *FOM* values of CFAR, PCP and the low-rank method were 0.81, 0.89 and 0.98, respectively. The results indicate that the low-rank method performs the best, followed by PCP, and the CFAR method performs the worst. Furthermore, six tracks of ships were obtained with location and time constraints. The consistency between the inversion velocity and AIS velocity was evaluated, and the mean error of velocity inversion was 0.12 m/s, with a mean relative error of 4.7%. The proposed method provides a new idea for radar target detection and tracking at sea.

ACKNOWLEDGMENT

The authors would like to thank the anonymous reviewers for their valuable comments and suggestions.

REFERENCES

[1] S. Watts, "ASV mark I, the first airborne maritime surveillance radar," *IEEE Aerosp. Electron. Syst. Mag.*, vol. 34, no. 8, pp. 50–61, Aug. 2019.
[2] C. Y. Chang, A. Woo, H. Forry, J. Sherman, M. Recht, R. Clark, and R. Levin, "HISAR-300: An advanced airborne multi-mission surveillance radar," in *Proc. IEEE Radar Conf. (RadarConf)*, Boston, MA, USA, Apr. 2019, pp. 1–6.
[3] D. Cerutti-Maori, J. Klare, A. R. Brenner, and J. H. G. Ender, "Wide-area traffic monitoring with the SAR/GMTI system PAMIR," *IEEE Trans. Geosci. Remote Sens.*, vol. 46, no. 10, pp. 3019–3030, Oct. 2008.
[4] H. Yan, R. Wang, F. Li, Y. Deng, and Y. Liu, "Ground moving target extraction in a multichannel wide-area surveillance SAR/GMTI system via the relaxed PCP," *IEEE Geosci. Remote Sens. Lett.*, vol. 10, no. 3, pp. 617–621, May 2013.
[5] J. Qian, W. U. Hao, and W. Yan, "Airborne multi-functional maritime surveillance radar system design and key techniques," *J. Radars*, vol. 8, no. 3, pp. 303–317, Mar. 2019.
[6] A. D. Jolly, "An airborne surveillance radar demonstrator," *Electron. Commun. Eng. J.*, vol. 12, no. 2, pp. 65–74, Apr. 2000.

[7] S. Watts, "The ASV 21 maritime surveillance radar," in *Proc. IEEE Radar Conf. (RadarConf)*, Seattle, WA, USA, May 2017, pp. 27–32.
[8] A. Damini, M. McDonald, and G. E. Haslam, "X-band wideband experimental airborne radar for SAR, GMTI and maritime surveillance," *IEE Proc. Radar, Sonar Navigat.*, vol. 150, no. 4, p. 305, Aug. 2003.
[9] L. Wang and L. Tan, "An airborne ocean surveillance SAR system and preliminary experiments," in *Proc. CIE Int. Conf. Radar (RADAR)*, Guangzhou, China, Oct. 2016, pp. 1–4.
[10] M. Kirscht, J. Mietzner, B. Bickert, J. Hippler, R. Zahn, and J. Boukamp, "An airborne radar sensor for maritime & ground surveillance and reconnaissance," in *Proc. EUSAR*, Berlin, Germany, 2014, pp. 1–4.
[11] M. Kirscht, A. Dallinger, J. Mietzner, B. Bickert, J. Hippler, and R. Zahn, "Advanced radar modes for airborne surveillance radars," in *Proc. 16th Int. Radar Symp. (IRS)*, Dresden, Germany, Jun. 2015, pp. 231–235.
[12] M. Kirscht, J. Mietzner, B. Bickert, A. Dallinger, J. Hippler, J. Meyer-Hilberg, R. Zahn, and J. Boukamp, "An airborne radar sensor for maritime and ground surveillance and Reconnaissance—Algorithmic issues and exemplary results," *IEEE J. Sel. Topics Appl. Earth Observ. Remote Sens.*, vol. 9, no. 3, pp. 971–979, Mar. 2016.
[13] S. Liu, Y. Ma, and Y. Huang, "Sea clutter cancellation for passive radar sensor exploiting multi-channel adaptive filters," *IEEE Sensors J.*, vol. 19, no. 3, pp. 982–995, Feb. 2019.
[14] Y. Feng, T. Shan, S. Liu, and R. Tao, "Interference suppression using joint spatio-temporal domain filtering in passive radar," in *Proc. IEEE Radar Conf. (RadarCon)*, Arlington, VA, USA, May 2015, pp. 1156–1160.
[15] B. Shi, C. Hao, C. Hou, X. Ma, and C. Peng, "Parametric Rao test for multichannel adaptive detection of range-spread target in partially homogeneous environments," *Signal Process.*, vol. 108, pp. 421–429, Mar. 2015.
[16] Y. Gao, G. Liao, S. Zhu, and D. Yang, "A persymmetric GLRT for adaptive detection in compound-Gaussian clutter with random texture," *IEEE Signal Process. Lett.*, vol. 20, no. 6, pp. 615–618, Jun. 2013.
[17] P.-L. Shui, M. Liu, and S.-W. Xu, "Shape-parameter-dependent coherent radar target detection in K-distributed clutter," *IEEE Trans. Aerosp. Electron. Syst.*, vol. 52, no. 1, pp. 451–465, Feb. 2016.
[18] G. V. Weinberg, "Constant false alarm rate detectors for Pareto clutter models," *IET Radar, Sonar Navigat.*, vol. 7, no. 2, pp. 153–163, Feb. 2013.
[19] X. Yu, X. Chen, Y. Huang, L. Zhang, J. Guan, and Y. He, "Radar moving target detection in clutter background via adaptive dual-threshold sparse Fourier transform," *IEEE Access*, vol. 7, pp. 58200–58211, 2019.
[20] E. Magraner, N. Bertaux, and P. Refregier, "Detection in gamma-distributed nonhomogeneous backgrounds," *IEEE Trans. Aerosp. Electron. Syst.*, vol. 46, no. 3, pp. 1127–1139, Jul. 2010.
[21] Z. Wang, Y. Wang, K. Duan, and W. Xie, "Subspace-augmented clutter suppression technique for STAP radar," *IEEE Geosci. Remote Sens. Lett.*, vol. 13, no. 3, pp. 462–466, Mar. 2016.
[22] J. Carretero-Moya, J. Gismero-Menoyo, A. Asensio-Lopez, and A. Blanco-Del-Campo, "Small-target detection in high-resolution heterogeneous sea-clutter: An empirical analysis," *IEEE Trans. Aerosp. Electron. Syst.*, vol. 47, no. 3, pp. 1880–1898, Jul. 2011.
[23] P.-L. Shui and Y.-L. Shi, "Subband ANMF detection of moving targets in sea clutter," *IEEE Trans. Aerosp. Electron. Syst.*, vol. 48, no. 4, pp. 3578–3593, Oct. 2012.
[24] X. Wang, E. Aboutanios, and M. G. Amin, "Slow radar target detection in heterogeneous clutter using thinned space-time adaptive processing," *IET Radar, Sonar Navigat.*, vol. 10, no. 4, pp. 726–734, Apr. 2016.
[25] Y. Li, Y. Yang, and X. Zhu, "Target detection in sea clutter based on multifractal characteristics after empirical mode decomposition," *IEEE Geosci. Remote Sens. Lett.*, vol. 14, no. 9, pp. 1547–1551, Sep. 2017.
[26] G. Du, "Detection of sea-surface radar targets based on fractal model," *Electron. Lett.*, vol. 40, no. 14, pp. 906–907, Jul. 2004.
[27] J. Hu, W.-W. Tung, and J. Gao, "Detection of low observable targets within sea clutter by structure function based multifractal analysis," *IEEE Trans. Antennas Propag.*, vol. 54, no. 1, pp. 136–143, Jan. 2006.
[28] S.-N. Shi and P.-L. Shui, "Sea-surface floating small target detection by one-class classifier in time-frequency feature space," *IEEE Trans. Geosci. Remote Sens.*, vol. 56, no. 11, pp. 6395–6411, Nov. 2018.
[29] P.-L. Shui, H.-W. Liu, and Z. Bao, "Range-spread target detection based on cross time-frequency distribution features of two adjacent received signals," *IEEE Trans. Signal Process.*, vol. 57, no. 10, pp. 3733–3745, Oct. 2009.
[30] L. Zuo, M. Li, X. Zhang, Y. Wang, and Y. Wu, "An efficient method for detecting slow-moving weak targets in sea clutter based on time–frequency iteration decomposition," *IEEE Trans. Geosci. Remote Sens.*, vol. 51, no. 6, pp. 3659–3672, Jun. 2013.
[31] Y. Zhang, S. Qian, and T. Thayaparan, "Detection of a manoeuvring air target in strong sea clutter via joint time-frequency representation," *IET Signal Process.*, vol. 2, no. 3, pp. 216–222, Sep. 2008.
[32] L. Wang, J. Tang, and Q. Liao, "A study on radar target detection based on deep neural networks," *IEEE Sensors Lett.*, vol. 3, no. 3, pp. 1–4, Mar. 2019.
[33] Z. Liu, D. K. C. Ho, X. Xu, and J. Yang, "Moving target indication using deep convolutional neural network," *IEEE Access*, vol. 6, pp. 65651–65660, 2018.
[34] N. del-Rey-Maestre, D. Mata-Moya, M.-P. Jarabo-Amores, P.-J. Gomez-del-Hoyo, and J.-L. Barcena-Humanes, "Artificial intelligence techniques for small boats detection in radar clutter. Real data validation," *Eng. Appl. Artif. Intell.*, vol. 67, pp. 296–308, Jan. 2018.
[35] Z. Zhang, Y. Xu, J. Yang, X. Li, and D. Zhang, "A survey of sparse representation: Algorithms and applications," *IEEE Access*, vol. 3, pp. 490–530, 2015.
[36] J. Wright, A. Ganesh, K. Min, and Y. Ma, "Compressive principal component pursuit," in *Proc. IEEE Int. Symp. Inf. Theory Proc.*, Cambridge, MA, USA, Jul. 2012, pp. 1276–1280.
[37] Y. Peng, A. Ganesh, J. Wright, W. Xu, and Y. Ma, "RASL: Robust alignment by sparse and low-rank decomposition for linearly correlated images," *IEEE Trans. Pattern Anal. Mach. Intell.*, vol. 34, no. 11, pp. 2233–2246, Nov. 2012.
[38] Y. Zhang and T. Xia, "In-wall clutter suppression based on low-rank and sparse representation for through-the-wall radar," *IEEE Geosci. Remote Sens. Lett.*, vol. 13, no. 5, pp. 671–675, May 2016.
[39] E. J. Candes, X. Li, and Y. Ma, "Robust principal component analysis?" *J. ACM*, vol. 58, no. 3, pp. 1–37, 2011.
[40] X. Zhou, C. Yang, and W. Yu, "Moving object detection by detecting contiguous outliers in the low-rank representation," *IEEE Trans. Pattern Anal. Mach. Intell.*, vol. 35, no. 3, pp. 597–610, Mar. 2013.
[41] H. Chen, M. Li, Z. Wang, Y. Lu, R. Cao, P. Zhang, L. Zuo, and Y. Wu, "Cross-range resolution enhancement for DBS imaging in a scan mode using aperture-extrapolated sparse representation," *IEEE Geosci. Remote Sens. Lett.*, vol. 14, no. 9, pp. 1459–1463, Sep. 2017.
[42] W. Li, J. Yang, and Y. Huang, "Keystone transform-based space-variant range migration correction for airborne forward-looking scanning radar," *Electron. Lett.*, vol. 48, no. 2, pp. 121–122, Jan. 2012.
[43] S. Geman and D. Geman, "Stochastic relaxation, Gibbs distributions, and the Bayesian restoration of images," *IEEE Trans. Pattern Anal. Mach. Intell.*, vol. PAMI-6, no. 6, pp. 721–741, Nov. 1984.
[44] B. Recht, M. Fazel, and P. A. Parrilo, "Guaranteed minimum-rank solutions of linear matrix equations via nuclear norm minimization," *SIAM Rev.*, vol. 52, no. 3, pp. 471–501, Jan. 2010.
[45] R. Mazumder, T. Hastie, and R. Tibshirani, "Spectral regularization algorithms for learning large incomplete matrices," *J. Mach. Learn. Res.*, vol. 11, pp. 2287–2322, Jan. 2010.
[46] J.-F. Cai, E. J. Candès, and Z. Shen, "A singular value thresholding algorithm for matrix completion," *SIAM J. Optim.*, vol. 20, no. 4, pp. 1956–1982, Jan. 2010.
[47] Y. Boykov, O. Veksler, and R. Zabih, "Fast approximate energy minimization via graph cuts," *IEEE Trans. Pattern Anal. Mach. Intell.*, vol. 23, no. 11, pp. 1222–1239, Nov. 2001.
[48] V. Kolmogorov and R. Zabih, "What energy functions can be minimized via graph cuts?" *IEEE Trans. Pattern Anal. Mach. Intell.*, vol. 26, no. 2, pp. 147–159, Feb. 2004.
[49] M. Zhen-qiu and C. Wei, "Angle measurement performance analysis and simulation of sum and difference phase-comparison monopulse radar," in *Proc. IET Conf. Publications*, Guilin, Guilin, 2009, pp. 1–6.
[50] W. L. Melvin, "A STAP overview," *IEEE Aerosp. Electron. Syst. Mag.*, vol. 19, no. 1, pp. 19–35, Jan. 2004.
[51] C. Cao, J. Zhang, and X. Zhang, "The analysis of ship target detection performance with C band compact polarimetric SAR," *Period. Ocean Univ. China*, vol. 47, no. 2, pp. 85–93, Feb. 2017.
[52] H. Esmaeili-Najafabadi, M. Ataei, and M. F. Sabahi, "Designing sequence with minimum PSL using Chebyshev distance and its application for chaotic MIMO radar waveform design," *IEEE Trans. Signal Process.*, vol. 65, no. 3, pp. 690–704, Feb. 2017.
[53] C. Cao, J. Zhang, J. Meng, X. Zhang, and X. Mao, "Analysis of ship detection performance with full-, compact-and dual-polarimetric SAR," *Remote Sens.*, vol. 11, no. 18, p. 2160, Sep. 2019.

CHENGHUI CAO received the B.S. degree in mathematics and the M.S. degree in applied mathematics from Qingdao Technological University, Qingdao, China, in 2014 and 2017, respectively. She is currently pursuing the Ph.D. degree in information and communication engineering with the Harbin Institute of Technology.

Her main research interests include radar target detection and sea clutter analysis.

JIE ZHANG received the B.S. and M.S. degrees in mathematics from Inner Mongolia University, Urumqi, China, in 1984 and 1987, respectively, and the Ph.D. degree in applied mathematics from Tsinghua University, Beijing, China, in 1993.

He is the Director of the Laboratory of Marine Physics and Remote Sensing, Ministry of Natural Resources, First Institute of Oceanography, Qingdao, China. He has a broad interest in marine physics and remote sensing applications. His research mainly focuses on the following: the SAR retrieval of ocean dynamics processes and the SAR detection of marine targets, ocean hyperspectral remote sensing, high-frequency surface-wave radar ocean detection techniques, and the integration of marine remote sensing application systems. He has served as a member of multiple domestic/international committees and a principal investigator/coinvestigator of many projects from the National Science Foundation of China, the State High-Tech Development Plan (863), and other funding agencies. He has been the supervisor of nearly 40 Ph.D. degree students and has published more than 200 articles.

JUNMIN MENG (Member, IEEE) received the B.S. degree in mathematics from Inner Mongolia Normal University, Urumqi, China, in 1996, the M.S. degree in applied mathematics from Inner Mongolia University, Urumqi, in 1999, and the Ph.D. degree in physical oceanography from the Ocean University of China, Qingdao, China, in 2002.

He is a Professor with the Laboratory of Marine Physics and Remote Sensing, Ministry of Natural Resources, First Institute of Oceanography, Qingdao. He is currently working on the development of algorithms determining marine parameters from microwave remote sensing.

XI ZHANG (Member, IEEE) received the B.S. degree in information systems from the Qingdao University of Science and Technology, Qingdao, China, in 2005, and the M.S. degree in signal and information processing and the Ph.D. degree in computer science from the Ocean University of China, Qingdao, in 2008 and 2011, respectively.

He is an Associate Professor with the Laboratory of Marine Physics and Remote Sensing, Ministry of Natural Resources, First Institute of Oceanography, Qingdao. His research interests include the microwave remote sensing of sea ice, the numerical modeling of sea ice scattering, and synthetic aperture radar data analysis. He participated in several land-based and airborne geoscientific field studies, among which a number of campaigns were related to sea ice studies in the Bohai sea.

XINGPENG MAO (Member, IEEE) was born in Liaoning, China, in 1972. He received the B.S. degree in radio electronics from Northeast Normal University, Changchun, China, in 1993, and the M.S. and Ph.D. degrees from the Harbin Institute of Technology, Harbin, China, in 1999 and 2004, respectively, all in electrical engineering.

He joined the Harbin Institute of Technology in 1993 as a Lecturer, working on the design and development of radar and other electronic systems. From 2005 to 2006, he was a Postdoctoral Fellow of the University of Waterloo, Waterloo, ON, Canada. He is currently a Professor with the Department of Electronics and Information Engineering, Harbin Institute of Technology. His current interests include signal processing in wireless communication and radars. He is a Senior Member of the Chinese Institute of Electronics.